Evaluations of the Spheroidal Particle Model for Describing Cloud Radar Depolarization Ratios of Ice Hydrometeors

SERGEY Y. MATROSOV

Cooperative Institute for Research in Environmental Sciences, University of Colorado Boulder, and NOAA/Earth System Research Laboratory, Boulder, Colorado

(Manuscript received 18 June 2014, in final form 14 November 2014)

ABSTRACT

Information on ice cloud particle nonsphericity is important for many practical applications ranging from modeling the cloud radiation impact to remote sensing of hydrometeor microphysical properties. Scanning cloud radars, which often measure depolarization ratio as a sole polarization variable, can provide a means for retrieving this information. The applicability of a spheroidal particle model (i.e., a regular ellipsoid that has two principal axes of the same length) is evaluated for describing depolarization properties of ice particles. It is shown that this simple model, which uses an aspect ratio as a single parameter characterizing particle nonsphericity, explains reasonably well the scatter of slant 45° linear depolarization ratio (SLDR) measurements versus direct estimates of the zenith direction backscatter enhancement observed during the Storm Peak Laboratory Cloud Property Validation Experiment (StormVEx) with the scanning W-band cloud radar (SWACR). Observed SLDR elevation angle patterns are also approximated reasonably well by this shape model. It is suggested that an SLDR difference between slant and zenith radar pointing can be used for prospective remote sensing methods of inferring particle aspect ratio from cloud radar depolarization measurements. Depending on mass–size relations, the value of this difference corresponding to median zenith reflectivity enhancement observed during StormVEx relates to aspect ratios of about 0.5 ± 0.2, which generally agrees with typical aspect ratios of ice particles. Expected aspect ratio retrieval uncertainties within the spheroidal shape model and the use of different types of radar depolarization ratio measurements are discussed. A correction for estimated zenith direction reflectivity enhancements due to particle nonsphericity is suggested.

1. Introduction

Information on ice hydrometeor types and shapes is important for modeling cloud radiative properties as part of climate and radiation studies (e.g., Avramov and Harrington 2010) and for remote sensing. This information can potentially be inferred from polarimetric radar data. Many cloud radars operating at Ka-band (~35 GHz) and W-band (~94 GHz) frequencies, including those from the U.S. Department of Energy (DOE) Atmospheric Radiation Measurement (ARM) program, directly measure one polarimetric variable [viz., depolarization ratio (DR)], thus limiting a number of potentially retrievable parameters describing particle shapes.

It has been shown experimentally with nearly collocated cloud radar and in situ ice particle observations that different types of Ka- and W-band DR values and their elevation angle trends can be used to differentiate among columnar and planar types of crystals and their aggregates (e.g., Matrosov et al. 2001, 2012; Reinking et al. 2002). Recently, Tyynelä and Chandrasekar (2014) discussed approaches to distinguish among different types of falling snow using multifrequency dual-polarization measurements. Microphysical in situ data (e.g., Korolev and Isaac 2003) show that pristine shapes (e.g., dendrites, needles) describe a relatively small fraction of observed particles, a majority of which have irregular nonspherical shapes. These authors also used an aspect ratio parameter to quantitatively describe particle nonsphericity. It will be useful for different application if information on such quantitative measure of particle shape can be derived from remote sensing measurements.

A simple shape model that accounts for general nonsphericity is the spheroidal model representing a regular ellipsoid whose two out of three axes are of the same length. The aspect ratio r in this model (i.e., the ratio of particle smallest and largest dimensions)

Corresponding author address: Sergey Y. Matrosov, R/PSD2, 325 Broadway, Boulder, CO 80305.
E-mail: sergey.matrosov@noaa.gov

DOI: 10.1175/JTECH-D-14-00115.1

describes a particle's degree of nonsphericity, while oblate–prolate spheroids are used to represent planar–columnar ice hydrometeor types. Using experimental data, this model has been previously shown to adequately describe radar dual-wavelength ratio (DWR) and differential reflectivity in ice clouds (e.g., Matrosov et al. 2005a; Hogan et al. 2012). A recent study with more sophisticated aggregate ice particle models and computational approaches (Leinonen et al. 2012) indicated that in some cases for larger particle populations resulting in high values of DWR spheroidal model may not provide consistency for DWR values over multiple radar wavelengths. However, as shown by these authors for other experimental cases, the spheroidal model can explain DWR radar observations while more sophisticated models cannot.

Recent studies with complex models (e.g., Petty and Huang 2010; Botta et al. 2011; Tyynelä et al. 2011) indicated also that for individual large ice particles, the use of shape models with homogeneous mixtures of ice and air can result in significant underestimation of backscatter cross sections. The backscatter errors are more pronounced for particles with larger size to wavelength ratios. For such particles it is important how the mass inside a particle is distributed. For many observed particle populations, however, larger particles contribute to the integral backscatter relatively little because of their small concentrations. As a result, the homogeneous spheroidal model backscatter is often in reasonable agreement with a range predicted by more sophisticated particle shapes (Liu 2008) and provides for larger particle populations such as snowfall (Matrosov 2007) W-band reflectivity values up to about 15 dBZ, which is close to largest observed values at this frequency band (e.g., Liu 2008). It has been also shown (Hogan and Westbrook 2014, their Fig. 5) that particle populations of more complex shape aggregates and spheroids of the same mass and aspect ratios provide similar W-band backscatter. While the differences between these two particle model backscatter generally increase with reflectivity, even for highest reflectivities (i.e., larger characteristic sizes) these differences are similar to the backscatter variability caused by a reasonable uncertainty in aspect ratios for the same particle model (e.g., 0.5 versus 0.6).

Since DR is often the only polarimetric variable available from cloud radars, it is important to evaluate if and how different particle model predictions correspond to observations. Tyynelä et al. (2011) compared theoretical vertical–horizontal linear depolarization ratio (HLDR) prediction from different models. They did not account for radar system cross coupling and their results indicate that HLDR for particle sizes smaller than 0.4 cm is less than about −22 dB, which would be often near the measurement noise since many cloud radars have the polarization cross-coupling level in the range of about −22 to −28 dB. An objective of this study was to assess a utility of the spheroidal model for describing depolarization caused by ice hydrometeors. This study uses observations at W band, which is the highest (i.e., the most challenging for modeling) frequency used by meteorological radars, using data collected by a scanning W-band ARM cloud radar (SWACR) in diverse ice cloud and precipitation conditions.

2. Theoretical considerations

Scatterer shape affects the polarization properties of measured radar returns, so polarimetric variables can be used for inferring particle shape information. Many cloud radars operating at millimeter wavelengths, including those from the ARM Program, transmit a single polarization signal and receive copolar and cross-polar components of the backscattered echo. The vector of voltages of these components (V_{co} and V_{cr}, correspondingly) in presence of unavoidable radar system cross coupling can be expressed as (e.g., Zrnić et al. 2010)

$$(V_{co}, V_{cr})^{T} = \mathbf{F}^{T}\mathbf{B}\mathbf{F}\mathbf{E}_{i} = \begin{pmatrix} F_{11} & F_{21} \\ F_{12} & F_{22} \end{pmatrix} \begin{pmatrix} B_{11} & B_{12} \\ B_{21} & B_{22} \end{pmatrix} \begin{pmatrix} F_{11} & F_{12} \\ F_{21} & F_{22} \end{pmatrix} (1,0)^{T}, \quad (1)$$

where the superscript ^{T} is the transpose sign; $\mathbf{F}$ and $\mathbf{B}$ represent the radar system cross coupling and target backscatter amplitude matrices, respectively; and the last term represents the transmitted unit electrical vector. For the traditional horizontal–vertical (h–v) polarization basis in the case of hydrometeor backscatter, the elements of the matrix $\mathbf{B}$ for a spheroid can be expressed as (e.g., Holt 1984)

$$B_{11} = B_{hh} = S_{hh}\cos^2\alpha + S_{vv}\sin^2\alpha, \quad (2a)$$

$$B_{12} = B_{21} = B_{hv} = 0.5(S_{vv} - S_{hh})\sin 2\alpha, \quad \text{and} \quad (2b)$$

$$B_{22} = B_{vv} = S_{vv}\cos^2\alpha + S_{hh}\sin^2\alpha, \quad (2c)$$

where α is the apparent canting angle (i.e., the angle between the projection of the hydrometeor axis zenith angle on the incident wave polarization plane and the vertical polarization vector) and S_{hh} and S_{vv} are the zero canting complex backscatter amplitudes along the unit vectors of the horizontal and vertical polarization, respectively. The normalizing terms are omitted as they do not influence radar variables that will be considered (i.e., reflectivity logarithmic differences and depolarization ratios). The matrix elements in Eq. (2) for particles, which are not canted in the polarization plane or are

oriented arbitrarily (i.e., without explicitly expressing dependence on α), can be calculated using the T-matrix method (e.g., Mishchenko et al. 1996) applicable to the "soft" spheroidal model. Calculations for typical particle size distributions using different available to the community versions of this method results in some relatively minor differences (less than a few tenths of 1 dB), which does not significantly affect results of this study. It should be noted also that certain computational limitations exist if the matrix elements S_{hh} and S_{vv} are expressed in terms of the scattering amplitudes along the spheroid principal axes (Holt 1984).

Equation (2) is written in the backscatter alignment (BSA) convention, where S_{hh} and S_{vv} generally have the same sign. Note that in the optical convention (Bohren and Huffman 1983), which is also widely used, they have the opposite signs (e.g., $S_{hh} = -S_{vv}$ for a sphere) and $B_{21} = -B_{12}$. The media transmission (e.g., differential phase on propagation) effects are neglected here because further comparisons are performed for short observational ranges (i.e., a few kilometers). Attenuation in dry ice is generally small (e.g., Matrosov 2007), and attenuation in atmospheric gases and in cloud liquid composed of small spherical drops is the same for both orthogonal polarizations, thus not affecting DR.

The backscatter matrix in the slant linear polarization basis $\mathbf{B}_{sl}$ can be obtained from the h–v backscatter matrix $\mathbf{B}_{hv}$ as

$$\mathbf{B}_{s1} = \mathbf{R}(-\gamma)\mathbf{B}_{hv}\mathbf{R}(\gamma), \tag{3}$$

where the rotation matrix $\mathbf{R}(\gamma)$ is given by

$$\mathbf{R}(\gamma) = \begin{pmatrix} \cos\gamma & \sin\gamma \\ -\sin\gamma & \cos\gamma \end{pmatrix}. \tag{4}$$

For the slant 45° ($\gamma = 45°$) polarization basis, which is sometimes used with cloud radars, rotating according to Eqs. (3) and (4) provides for the matrix elements in Eq. (1),

$$B_{11} = 0.5S_{hh} + 0.5S_{vv} + (S_{hh} - S_{vv})\sin\alpha\cos\alpha, \tag{5a}$$

$$B_{12} = B_{21} = 0.5(S_{hh} - S_{vv})\cos 2\alpha, \quad \text{and} \tag{5b}$$

$$B_{22} = 0.5S_{hh} + 0.5S_{vv} - (S_{hh} - S_{vv})\sin\alpha\cos\alpha. \tag{5c}$$

The backscatter matrix in the circular polarization basis $\mathbf{B}_c$ can be obtained from the h–v backscatter matrix $\mathbf{B}_{hv}$ as

$$\mathbf{B}_c = \mathbf{C}^{-1}\mathbf{B}_{hv}\mathbf{C}, \tag{6}$$

where the matrix $\mathbf{C}$ is given by

$$\mathbf{C} = 0.5^{1/2}\begin{pmatrix} 1 & 1 \\ j & -j \end{pmatrix}. \tag{7}$$

The corresponding matrix elements for circular polarization are

$$B_{11} = 0.5(S_{hh} - S_{vv})\exp(-2j\alpha), \tag{8a}$$

$$B_{12} = B_{21} = 0.5(S_{hh} + S_{vv}), \quad \text{and} \tag{8b}$$

$$B_{22} = 0.5(S_{hh} - S_{vv})\exp(2j\alpha), \tag{8c}$$

where $j^2 = -1$. As seen from Eq. (8) the main power return in the circular polarization basis comes in the cross-polarization receiver channel.

The trigonometric functions of the apparent canting angle α are related to the particle axis orientation zenith θ and azimuthal ϕ angles and radar elevation angle χ in the following way (Holt 1984):

$$\cos\alpha\sin\psi = \cos\theta\cos\chi + \sin\theta\sin\chi\cos\phi, \tag{9a}$$

$$\sin\alpha\sin\psi = \sin\theta\sin\phi, \quad \text{and} \tag{9b}$$

$$\cos\psi = \cos\theta\sin\chi - \sin\theta\cos\chi\cos\phi, \tag{9c}$$

where ψ is the particle axis orientation angle with respect to the propagation direction of the incidence electromagnetic wave. Note that θ is the "true" canting angle.

It can be assumed (Zrnić et al. 2010) that, in the radar system cross-coupling matrix $F_{11} = F_{22}$ and after the normalization of this matrix by the value of the diagonal elements, the transmit/receive isolation can be expressed by a small, complex cross-talk term ε (Bringi and Chandrasekar 2001, chapter 6.1) representing off-diagonal elements of this matrix. The depolarization ratio in the linear bases is then can be expressed as

$$\mathrm{DR} = 10\log_{10}(\langle|V_{cr}|^2\rangle/\langle|V_{co}|^2\rangle) = 10\log_{10}[\langle|B_{12} + \varepsilon(B_{11} + B_{22}) + \varepsilon^2 B_{12}|^2\rangle/\langle|B_{11} + 2\varepsilon B_{12} + \varepsilon^2 B_{22}|^2\rangle], \tag{10}$$

where angular brackets denote integration over hydrometer size and canting angle distributions. Small terms containing $\varepsilon^2 B_{12}$ in the nominator and $\varepsilon^2 B_{22}$ in the denominator can be safely neglected. The second term

in the denominator also can be neglected because for most practical cases the copolar echo signals are much stronger than cross-polar signals and $|B_{11}| \gg 2|\varepsilon B_{12}|$. These simplifications yield

$$\mathrm{DR} \approx 10\log_{10}\{(\langle|B_{12}|^2\rangle + |\varepsilon|^2\langle|B_{11}+B_{22}|^2\rangle + 2\mathrm{Re}[\langle(B_{11}+B_{22})B_{12}^*\rangle\varepsilon])/\langle|B_{11}|^2\rangle\}, \quad (11)$$

where * is the complex conjugate sign. The third term in the numerator of Eq. (11) averages to zero because of reflection symmetry (e.g., Bringi and Chandrasekar 2001, chapter 6.1) providing further simplification,

$$\mathrm{DR} \approx 10\log_{10}[(\langle|B_{12}|^2\rangle + |\varepsilon|^2\langle|B_{11}+B_{22}|^2\rangle)/\langle|B_{11}|^2\rangle]. \quad (12)$$

Note that Eq. (12) is written for the linear polarization basis. Substitutions in the Eq. (12) $B_{11} + B_{22} \rightarrow 2B_{12}$ and $B_{11} \leftrightarrow B_{12}$ provide estimates of DR in the circular polarization basis.

It is essential to evaluate the performance of radar systems for depolarization measurements (i.e., to estimate $|\varepsilon|^2$) because observed DR values are often quite different from intrinsic DR values expected from a "perfect" radar system, which are given by Eq. (12) when assuming $|\varepsilon|^2 = 0$ {i.e., $\mathrm{DR} \approx 10\log_{10}[\langle|B_{12}|^2\rangle/\langle|B_{11}|^2\rangle]$}. The value of $|\varepsilon|^2$ for a given linear polarization basis can be estimated by taking measurements in a cloud of spherical hydrometeors for which $B_{11} = B_{22}$ and $B_{12} = 0$. For such targets $\mathrm{DR} = \mathrm{DR}_{\min} = 10\log_{10}(4|\varepsilon|^2)$.

For the slant 45° SWACR configuration, which was used during the Storm Peak Laboratory Cloud Property Validation Experiment (StormVEx) deployment (Mace et al. 2010), it was established during measurements in drizzle that minimum observable depolarization, which characterizes system polarization cross talk $\mathrm{DR}_{\min}$ is about −21.8 dB, so the value of $|\varepsilon|$ was estimated as 0.0406 (Matrosov et al. 2012). The estimation of the cross-talk effects allows for modeling polarization properties of radar returns tuned for a particular radar system. Modeling using the relation for the intrinsic depolarization ratio can result in biased DR estimates, which will not generally correspond to observed values (especially for lower depolarizations).

The slant 45° linear polarization basis in StormVEx was chosen because earlier K_a-band radar data indicated the advantage of using circular and slant linear DR compared to traditional horizontal–vertical linear DR for the purpose of ice particle habit identification (e.g., Reinking et al. 2002). This advantage is mainly due to much stronger dependence of the traditional *h–v* linear basis DR to particle orientations and lower echoes in the "weak" receiving channel for this basis compared to the circular and slant linear polarization bases. While the circular polarization has some advantages over the slant 45° linear polarization for particle shape estimates (Matrosov et al. 2001), the latter one was chosen for the SWACR in StormVEx because of easier implementation.

3. Comparisons of modeled and observed cloud radar depolarization measurements

a. Particle mass–size relations and aspect ratios

Particle mass (along with its shape and size) is an essential parameter that defines hydrometeor scattering properties. The mass m is typically related to the size D. A number of power-law relations of the type

$$m = aD^b, \quad (13)$$

where a and b are empirical coefficients, have been suggested in the literature for different ice particle types (e.g., Mitchell 1996). Typically the exponent b in *m–D* relations is around 2 while the coefficient a varies more significantly, and D is expressed in terms of particle major dimension as a diameter. One such relation with $a = 7.38 \times 10^{-11}$ and $b = 1.9$ (when m is grams and D is in microns), which is widely used in different studies, was evaluated by Brown and Francis (1995), who found that it adequately describes independent measurements of ice content.

Figure 1a shows the Brown and Francis (1995) relation and its variations with the coefficient being half and twice the original value (i.e., 3.69×10^{-11} and 1.47×10^{-10}) and also the relation from Matrosov (2007) that was used here for modeling. The latter relation was suggested for aggregates, and it provides a continuous transition from particle bulk densities typically found in nonprecipitating ice clouds to densities of larger snowflakes (e.g., Brandes et al. 2007). The range of the coefficient a values considered here accounts for potential variability in this coefficient and covers a refinement factor of 1.25 suggested by Hogan et al. (2012) to better match the maximum particle dimension and the size measured by Brown and Francis (1995).

Particle bulk densities corresponding to the *m–D* relations from Fig. 1a are shown in Fig. 1b for the assumption of the oblate spheroid shape and the aspect ratio $r = 0.6$, which is around the average value observed in actual ice clouds (Korolev and Isaac 2003). Note that for densities with different particle aspect ratio assumptions, the data in Fig. 1b should be multiplied by a factor of $0.6/r$. The data in this figure and calculations

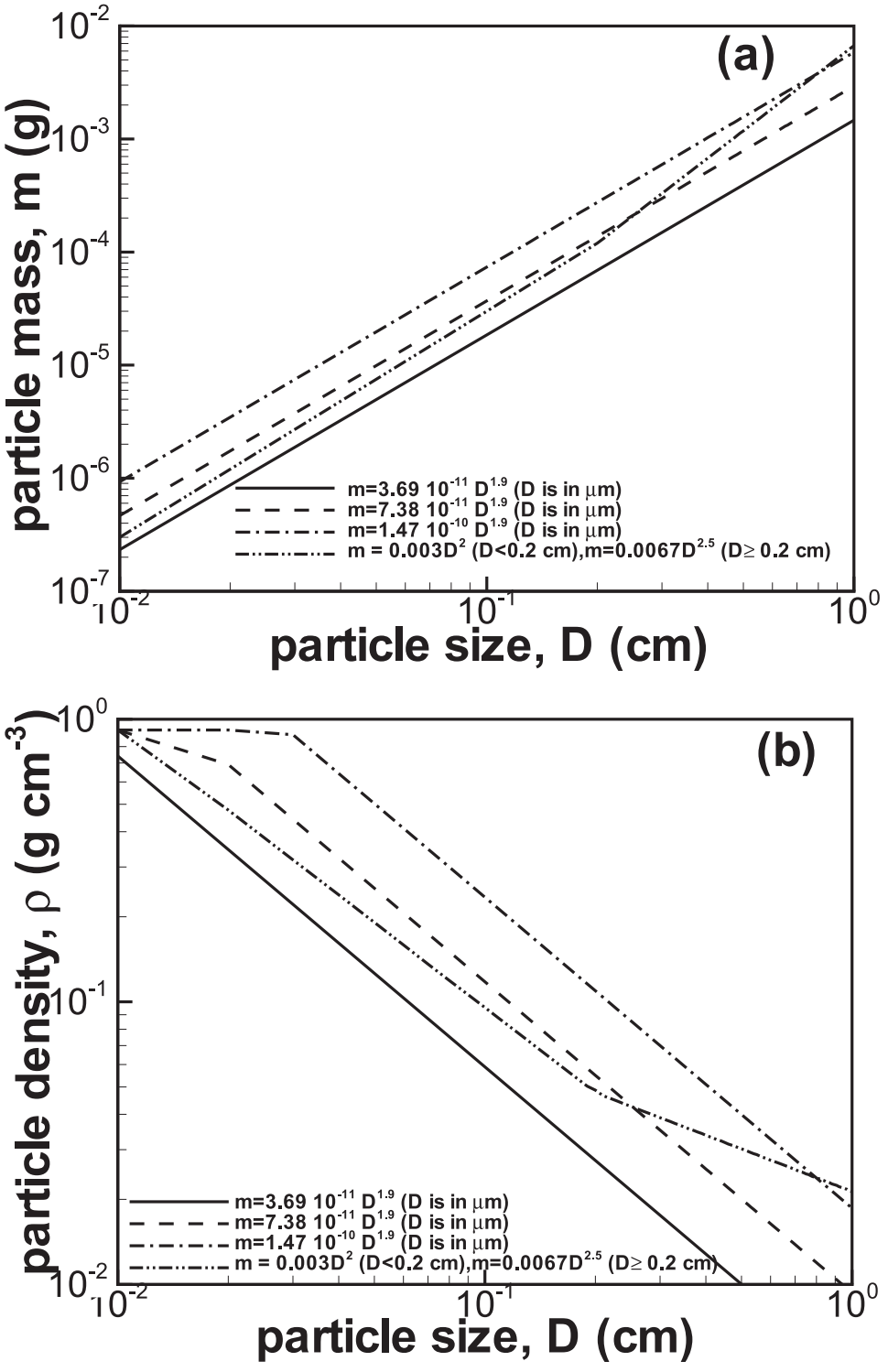

FIG. 1. (a) Different mass–size relations for ice particles and (b) corresponding densities of oblate spheroidal particles with an aspect ratio of 0.6.

were capped at the solid ice density of 0.91 g cm^{-3}, which results in curve cusps at higher density end. The cusp in curve 4 results from differing m–D relations for $D \leq 0.2$ cm and $D > 0.2$ cm. For smaller r values, the densities correspond well to the bulk densities of pristine dendrites and stellars as given in Pruppacher and Klett (1978) (e.g., around 0.5–0.7 g cm^{-3} for 1-mm particles with $r \sim 0.05$–0.1). Particle bulk densities were used to calculate refractive indices using the Maxwell Garnett mixing rule (Garnett 1904) with spherical solid ice inclusions into the air matrix.

In model calculations particle aspect ratios varied from 1 (i.e., spheres) to 0.2. Smaller aspect ratios, while likely being more appropriate for pristine habits such as dendrites and plates, were not modeled since the T-matrix method for calculating scattering amplitudes of such particles becomes increasingly unstable especially for larger sizes. Particle populations in this study were modeled using the exponential distribution $N(D) = N_0 \exp(-3.67D/D_0)$, which usually describes well concentrations of particles contributing most to the total reflectivity (Heymsfield et al. 2008). For relative variables such as DR and reflectivity differences in the decibel scale, the intercept of the exponential distribution is not important, so a single distribution parameter, the median volume particle size D_0, was considered here. Because of aerodynamic forcing, particles are on average oriented with their major dimensions in the horizontal plane (i.e., the mean true canting angle $\theta_{\text{mean}} = 0°$). Typical standard deviations of θ (σ_θ), which describes particle flutter, for dendrite-type oblate particles are about 8°–9°, as independent measurements based on different polarimetric radar variables indicate (Matrosov et al. 2005b; Melnikov and Straka 2013). It is assumed hereafter that the distribution of particle axes is Gaussian with respect to the zenith angle θ and random with respect to the azimuthal angle φ. The minimum and maximum sizes in integration were 25 μm and 1 cm, respectively, though for typical size distributions observed during StormVEx the largest particles generally contributed very little to integral backscatter (e.g., 50% variations in minimum and maximum integration limits resulted in modeled radar variable differences that were generally within a few tenths of 1 dB).

b. *Different radar depolarization ratios*

The StormVEx dataset (Matrosov et al. 2012; Marchand et al. 2013) indicated that a majority of the measurements were indicative of planar crystal habits when depolarization ratios were generally increasing from the minimal values observed around the zenith direction, which were usually near the level determined by the system cross coupling, toward higher values at slant viewing. Preliminary oblate spheroid modeling results were generally able to replicate such behavior of depolarization ratios for planar-type particles (Matrosov et al. 2012). A typical dominance of planar-type particles is also consistent with the results of Hogan et al. (2012), who, for a different dataset, showed that the oblate spheroid model was generally successful in explaining observed differential reflectivity patterns. Given this evidence the focus of the current study is on considering oblate-type particles as they typically dominate signals, even though a small number of events with dominant columnar (i.e., prolate-type) particles were observed during the StormVEx field project (Matrosov et al. 2012; Marchand et al. 2013).

For $\text{DR}_{\text{min}} = -21.8$ dB, Fig. 2a shows an example of modeled and observed elevation angle dependences of different depolarization ratios including traditional linear depolarization ratio when horizontal polarization is transmitted (HLDR), slant 45° linear depolarization ratio (SLDR), and circular depolarization ratio (CDR). The differences between HLDR and CDR (or SLDR) are more pronounced for particles that have higher degree of nonsphericity. For aspect ratios $r = 0.3$ in Fig. 2, these differences are rather clear. It can be seen that for modest values of σ_θ, CDR and SLDR are similar (although CDR is generally higher) and do not significantly depend on particle flutter σ_θ given that this flutter remains relatively modest. Note that CDR and SLDR are identical for noncanted hydrometeors as it could be seen from comparing Eqs. (5) and (8). In contrast to SLDR and CDR, HLDR values are very low and there is significant variability depending on σ_θ. For $\text{DR}_{\text{min}} = -21.8$ dB and $\sigma_\theta < 15°$, expected HLDR values are barely detectable even at slant viewing. Modeling using the spheroidal shapes approximate observed DR trends quite well, although as indicated by Matrosov et al. (2012) different sets of characteristic particle sizes–densities and aspect ratios can provide similar DR elevation angle patterns. More experimental examples of SWACR measurements and theoretical estimates of SLDR for a wide range of particle aspect ratios are presented by Matrosov et al. (2012) and Marchand et al. (2013).

Figure 2b shows the depolarization ratio elevation angle relations for a better cross-polarization isolation of the radar system with $\text{DR}_{\text{min}} = -28$ dB. This isolation level was characteristic for the SWACR when it was operated in the traditional h–v polarization basis. The SWACR conversion from the h–v polarization scheme to the slant 45° scheme inadvertently resulted in a loss in the system cross-polar isolation (i.e., −21.8 dB vs −28 dB). It can be seen from Fig. 2b that for

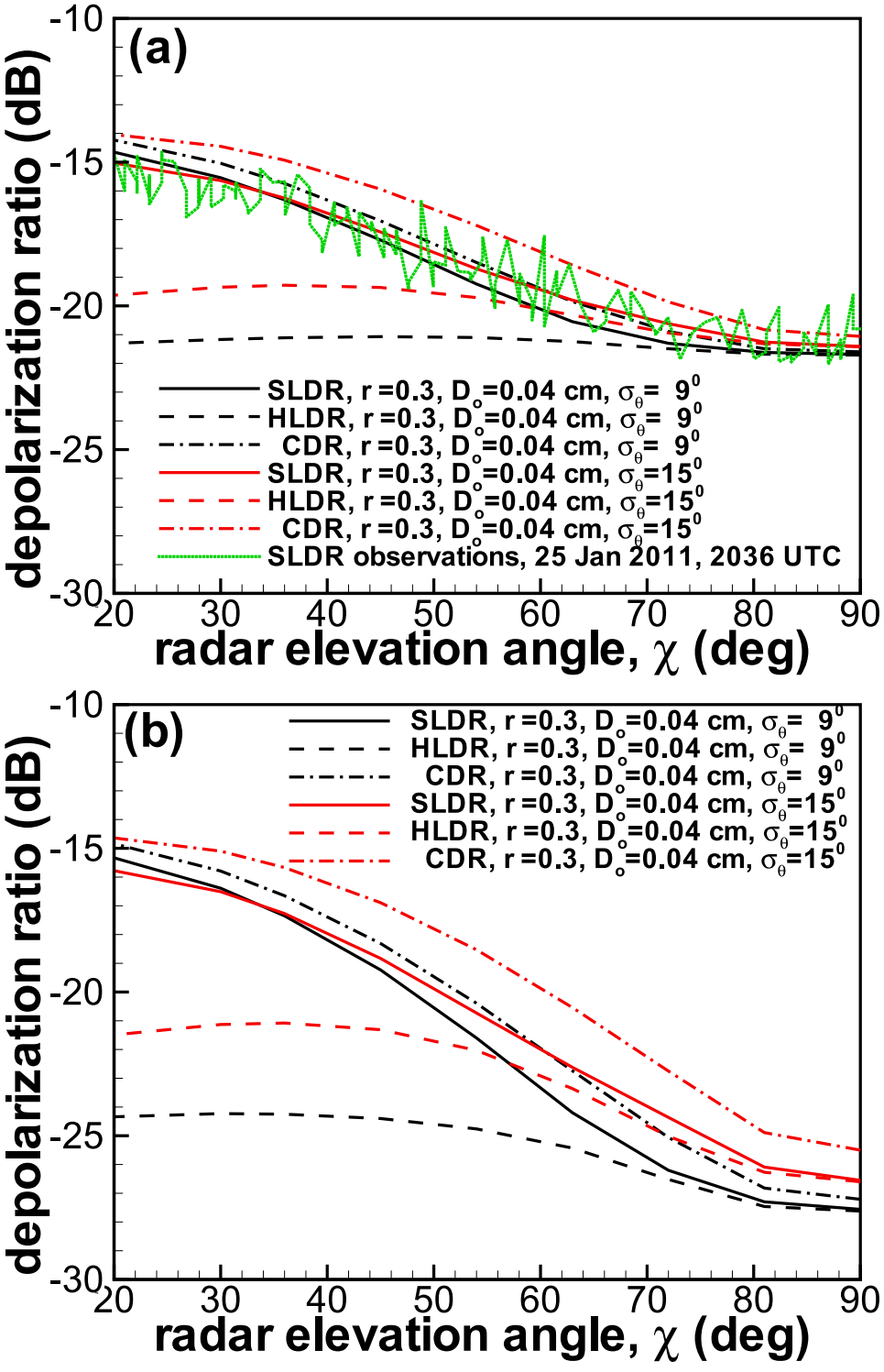

FIG. 2. Comparisons of model results of different depolarization ratio elevation angle dependencies with (a) observations for the SWACR crosstalk of −21.8 dB and (b) modeling results assuming the −28 dB crosstalk. The *m*–*D* relation from Brown and Francis (1995) and a particle aspect ratio $r = 0.3$ were assumed.

$DR_{min} = -28$ dB HLDR values could be better detectable (given that the cross-polarized signals are above the noise level), though there is still quite a strong dependence of HLDR on hydrometeor flutter σ_θ.

c. *Intercomparisons of model and observed SLDR–reflectivity enhancement relations*

As depolarization ratios, copolar reflectivity of oriented nonspherical hydrometeors Z_{co} depends on the direction of viewing. Changes in observed Z_{co} as a function of radar elevation angle are particularly large at W band, which is explained, in part, by non-Rayleigh scattering effects (Matrosov et al. 2005a). Differences between zenith and slant viewing values of Z_{co} during StormVEx were as large as about 12 dB during some events when single dendritic and/or plate crystals were a dominant particle habit (e.g., Matrosov et al. 2012; Marchand et al. 2013). While the oblate spheroidal model was able to generally predict patterns of the off-zenith reflectivity decrease (Matrosov et al. 2012), the meaningful comparisons were hampered by the fact that attenuation due to supercooled liquid water and atmospheric gases, while not a factor for depolarization measurements, generally enhances the magnitude of reflectivity decreasing trends.

Marchand et al. (2013) analyzed the StormVEx SWACR dataset selecting cases with relatively homogenous cloud conditions. For such cases, they corrected for attenuation effects using a symmetry of the range–height indicator (RHI) scan measurements and determined observational estimates of nonattenuated values of the reflectivity zenith enhancement ΔZ_{co}, which is defined as the logarithmic difference between reflectivities in the zenith ($\chi = 90°$) and slant ($\chi \approx 25°$–$35°$) directions. Values of ΔZ_{co} estimated from observations were found to strongly correlate (the correlation coefficient being 0.79) with the observed SLDR differences between zenith and slant viewing. A specific difference

$$\Delta\text{SLDR} = \text{SLDR}(90°) - \text{SLDR}(45°) \qquad (14)$$

was considered in the Marchand et al. (2013) study to relate observational values of ΔSLDR and ΔZ_{co} (their Fig. 5). The corresponding best linear fit is

$$\Delta Z_{co}(\text{dB}) = -1.14\Delta\text{SLDR} + 0.77. \qquad (15)$$

StormVEx estimates of ΔZ_{co} and ΔSLDR, which are largely free of attenuation effects, present a convenient dataset for testing a spheroidal particle model. Theoretical values of ΔZ_{co} and ΔSLDR were calculated using this model and the mass–size relations shown in Fig. 1. The attenuation-free reflectivity enhancements were estimated using Eq. (5a) from the expression

$$\Delta Z_{co} = 10\log_{10}[\langle|B_{11}(90°)|^2\rangle/\langle|B_{11}(30°)|^2\rangle]. \qquad (16)$$

For the oblate spheroid particle model, Fig. 3 shows the results of simulations of the correspondence between ΔZ_{co} and ΔSLDR. The ΔSLDR computations were performed using Eqs. (12) and (5) assuming the mass–size relations shown in Fig. 1 and three different values of the median volume particle size (0.04, 0.08, and 0.12 cm). Such characteristic distribution sizes were typical during StormVEx observations according to the measurements from Droplet Measurement Technologies (DMT) cloud and precipitation measurement probes that were part of the StormVEx instrument suite.

Although the particle orientation flutter for data in Fig. 3 was assumed to be $\sigma_\theta = 9°$, there is little variation of results when σ_θ varies between 0°, which corresponds to particle alignment with the major dimension in the horizontal plane, and about 15°. While the flutter for smaller particles could be higher, the observed variables, because of the nature of radar measurements, are more influenced by larger particles. The data that correspond to different values of aspect ratio r change along the curves depicted in Fig. 3 (spheres correspond to the graph origin (i.e., $\Delta Z_{co} = \Delta\text{SLDR} = 0$ dB). Data points for aspect ratios of 0.2 correspond to the end of the curves in this figure.

The area of measurement data scatter between observed values of ΔZ_{co} and ΔSLDR from Marchand et al. (2013) is also shown in Fig. 3. While this scatter area is rather large, about 90% of all data points were characterized by $\Delta Z_{co} < 6.4$ dB and belong to the lower part of Fig. 3, where the theoretical curves are located. The data area with larger ΔZ_{co} values, which is not generally covered by theoretical curves, generally corresponds to particles with very high degree of nonsphericity. Such particles were not modeled here because of the T-matrix method application restrictions mentioned above. As seen from Fig. 3, for the given mass–size relations and ΔSLDR values, particle populations with larger D_0 are expected to produce more significant zenith reflectivity enhancements.

As the aforementioned comparisons between measurements and modeling results show, the theoretical estimates of the correspondence between ΔZ_{co} and ΔSLDR generally fall within the range of observed quantities when reasonable assumptions about particle aspect ratios and mass–size relations are made. These results indicate that a spheroidal particle model may satisfactorily describe the depolarization properties and corresponding zenith direction backscatter enhancements observed in ice clouds and precipitation, at

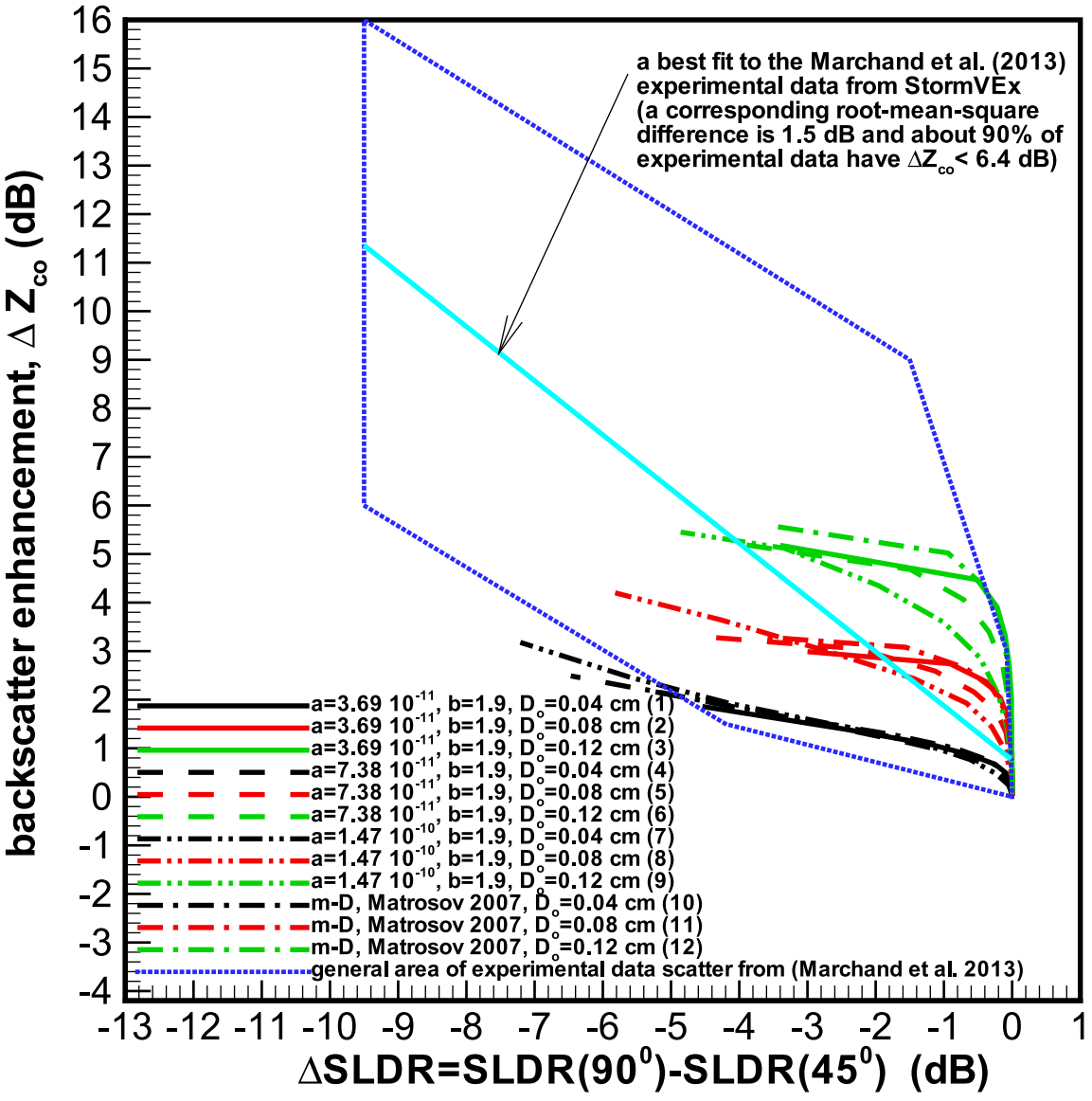

FIG. 3. Simulations of backscatter enhancement vs SLDR difference for spheroidal particle model for different mass–size relations and aspect ratio assumptions. Aspect ratio change along the curves shown from 1 at the (0, 0) point to 0.2 at the end of each individual curve.

least for hydrometeor size distributions with not very large particle characteristic sizes. Since the spheroidal model also describes particle nonsphericity using a single aspect ratio parameter, it is convenient to describe particles using this model. While such a description is obviously a certain simplification, particle shapes are often diverse and irregular; thus, it is not generally clear without further detailed studies if the use of particular more sophisticated nonpristine particle models can adequately describe the multiplicity of real shapes. Such models, however, are likely to be more appropriate for particles with larger size parameters. Future research, which is outside the scope of this study, should include comparisons of observed and theoretical radar depolarization ratios obtained with different particle models and computational techniques with accounting for polarimetric cross coupling, which affects these ratios in a significant way.

4. Potential for inferring particle aspect ratio from radar depolarization measurements

It can be concluded from Fig. 3 that the observed quantities can be described using different mass–size relations and aspect ratios. The aspect ratio estimates are needed for better representation of ice hydrometeors

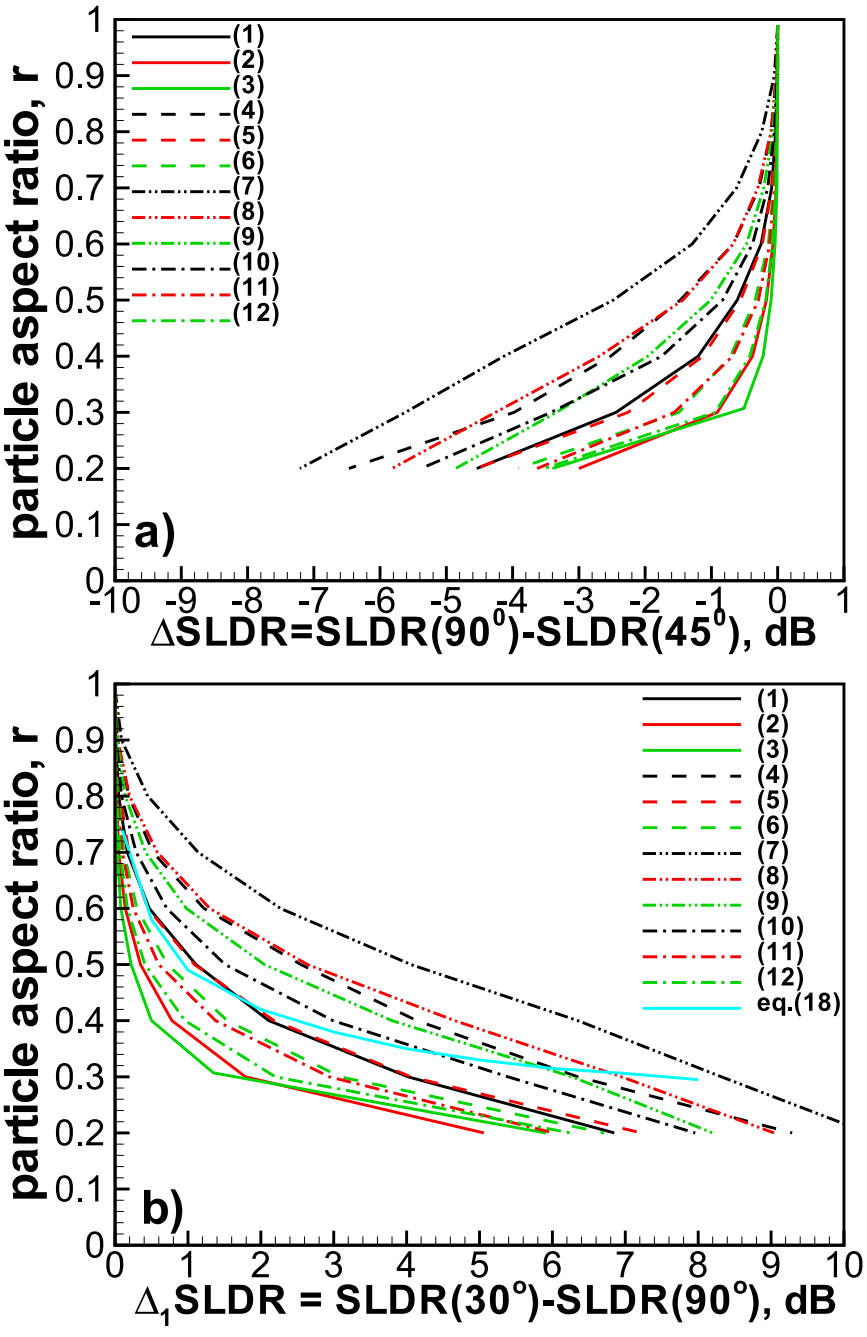

FIG. 4. Relations between particle aspect ratio and SLDR slant vs zenith viewing differences [(a) 90° vs 45° and (b) 30° vs 90°] for different mass–size relations and characteristic particle sizes. Numbers for combinations of m–D relations and D_0 are the same as in Fig. 3.

in cloud and climate models and also for enhancements of remote sensing methods that typically simply assume particle shapes. It is instructive to briefly evaluate potentials for particle aspect ratio retrievals using depolarization measurements in a framework of the simplified spheroidal model. The measurements using slant 45° linear or circular polarizations are suitable for this purpose, since they depend on the particle flutter parameter (i.e., σ_θ) relatively insignificantly. Since implementation of the slant 45° linear polarization is generally easier to perform in practice, the use of SLDR measurements is analyzed here.

Figure 4a shows particle aspect ratio r as a function of ΔSLDR for mass–size relation assumptions from Fig. 1

and different values of D_0. The median reflectivity enhancement measured during StormVEx was 2.4 dB, which corresponds to the observational value ΔSLDR of about −1.4 dB (Marchand et al. 2013). For the mass–size relation with coefficients used by Brown and Francis (1995) and for a median volume particle size of 0.04 cm, the corresponding value of r is approximately 0.5, which is not significantly different from the mean value from a large experimental aircraft-based dataset (Korolev and Isaac 2003). Given the data scatter provided by different curves in Fig. 4a, an aspect ratio uncertainty of at least 0.2 can be expected.

The range of SLDR changes is greater if depolarization at more slant viewing than 45° is compared to the zenith values, so the ''depolarization difference signal,'' which is used for aspect ratio estimations, is stronger. To illustrate this fact Fig. 4b shows relations between r and Δ_1SLDR defined as a positive difference between SLDR at radar elevation angles $\chi = 30°$ and 90°,

$$\Delta_1\mathrm{SLDR} = \mathrm{SLDR}(30°) - \mathrm{SLDR}(90°). \qquad (17)$$

Analyzing the data in Fig. 4b can provide some measure of errors that can be expected when estimating particle aspect ratios under the oblate spheroidal model when there are factor of 2 uncertainties in m–D relations and the distribution characteristic size. For example, Δ_1SLDR of about 2 dB (i.e., the ΔSLDR value of approximately −1.4 dB), which corresponds to the median value of the zenith reflectivity enhancement observed in StormVEx, can be produced by particles with aspect ratios r ranging from about 0.3 to 0.65. If Δ_1SLDR is greater than about 4 (8) dB, particles are expected to have r values less than about 0.5 (0.3). The larger aspect ratios (i.e., more spherical particles) for a given Δ_1SLDR value generally correspond to denser particles. For $\Delta_1\mathrm{SLDR} < 6$ dB, a mean power-law relation approximating a set of curves in Fig. 4b (for the StormVEx SWACR configuration) is given as

$$r \approx 0.47(\Delta_1\mathrm{SLDR})^{-0.19}, \qquad (18)$$

which is also depicted in Fig. 4b. It can be seen from this figure that that the power-law relation is not approximating results quite well at higher Δ_1SLDR values, so the use of actual model calculations might be needed for estimating aspect ratios less than about 0.3.

The particle mass–size relation and aspect ratio are the main properties that determine the magnitude of the SLDR change between slant and zenith viewing. The orientation flutter parameter σ_θ (given that σ_θ is relatively small) influences these changes to a significantly lesser extent. The median volume size of the distribution D_0 influences SLDR through dependence of particle bulk density on its size and also through non-Rayleigh scattering effects. Under the spheroidal model, the effective density of the distribution ρ_e, which is different from individual particle bulk densities shown in Fig. 1b, similarly to Heymsfield et al. (2004), can be defined as the ratio of cloud ice water content (IWC) to the total physical volume of particles in a unit volume of air. For the mass–size relations and particle characteristic sizes D_0 shown in Fig. 3, Fig. 5 depicts effective density of particle distributions as a function of particle aspect ratio.

The experimental data of Heymsfield et al. (2004) indicate that for the assumed spherical shape, which is equivalent to the assumption of $r = 1$ in Fig. 5, ρ_e mostly varies from about 0.04 to 0.7 g cm^{-3} (based on their ARM research aircraft flights) if $\Lambda \approx 3.67/D_0 > 10$ cm^{-1}. These experimental data on effective density of particle populations correspond well to the model values of this study in Fig. 5. For smaller aspect ratios, the effective density increases as the same mass is prescribed to smaller volumes.

The Fig. 5 data show that particle property assumptions corresponding to curves 1 and 9 (also 2 and 12) are characterized by similar effective densities. The Δ_1SLDR and ΔSLDR values at various aspect ratios for corresponding assumptions, however, are different (see Fig. 4). These differences manifest the characteristic size influences on SLDR changes, since the effective densities of these particle populations are approximately the same. The expected variability of Δ_1SLDR due characteristic size changes is, however, relatively modest. From comparing curves 1 and 9 in Fig. 4b, it can be seen that it is approximately 1–2 dB as D_0 changes as a factor of 3.

5. Zenith reflectivity enhancement

The zenith (or nadir) reflectivity increase due to the presence of nonspherical ice particles is a factor that needs to be accounted for when applying millimeter-wavelength radar-based remote sensing techniques that use vertical beam measurements for retrievals of microphysical parameters in ice clouds and precipitation. Of important practical interest is the reflectivity increase/enhancement compared to that of equal-mass spherical particles because the spherical particle assumption for microphysical retrievals is still used in a number of algorithms (e.g., Austin et al. 2009). Marchand et al. (2013) quantified the W-band zenith reflectivity enhancement ΔZ_{co} (relative to reflectivity at slant viewing at about 30°) based on the StormVEx observational dataset. When estimating ΔZ_{co} from radar data, their assumption was that observed reflectivity at slant viewing is similar to that of the spherical particles

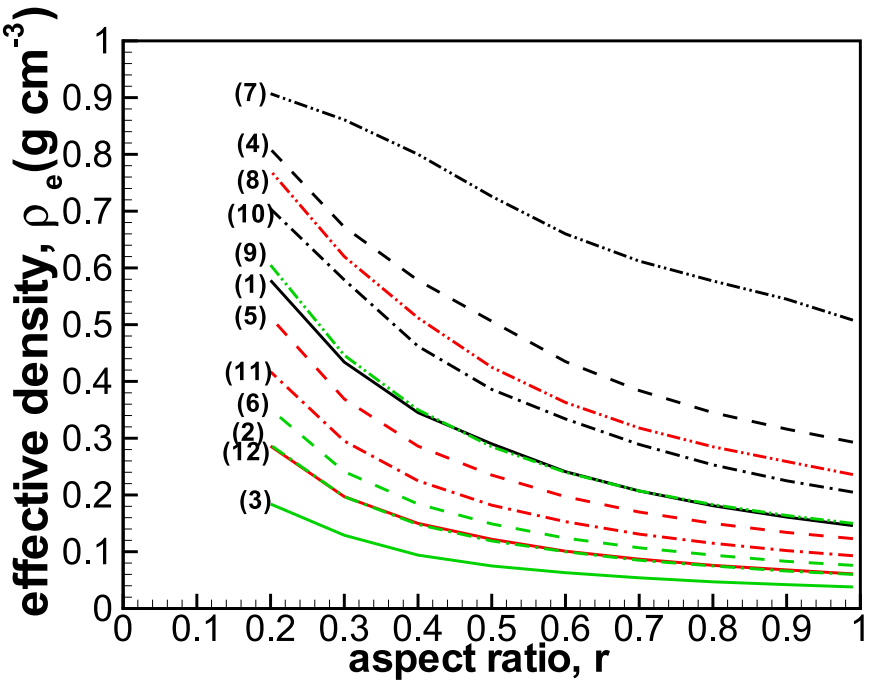

FIG. 5. Effective bulk densities of particle populations as a function of aspect ratio. Curve numbers correspond the mass–size relations and D_0 values in Fig. 3.

of the same mass. As discussed previously, these authors found from StormVEx observations that there is good correlation between Z_{co} and ΔSLDR expressed by the best linear fit given by Eq. (15).

One factor here is that, for the slant 45° linear polarization used by the SWACR during StormVEx, the reflectivity enhancement is different from the reflectivity enhancement that would be observed if the conventional horizontal polarization reflectivity measurements were used. Another factor to consider when accounting for zenith/nadir reflectivity enhancement is that the reflectivity of nonspherical particles at slant viewing is not generally equal to that of the spheres of the same mass even though the spherical–nonspherical reflectivity difference is smaller at slant viewing (~30°) than at zenith viewing. For practical purposes of microphysical retrievals, it would be useful to know what zenith reflectivity enhancement $\Delta_1 Z_{co}$ relative to spherical particles of the same mass and same maximum dimension could be expected for conventional vertical beam measurements when a ΔZ_{co} value was observed with the SWACR in the StormVEx configuration. The quantity $\Delta_1 Z_{co}$ was estimated using the expression

$$\Delta_1 Z_{co}(\mathrm{dB}) = 10\log_{10}[\langle|B_{11}(90°)|^2\rangle/\langle|B_{11}(r=0)|^2\rangle], \tag{19}$$

where $B_{11}(90°)$ and $B_{11}(r = 0)$ were calculated using (5a) for nonspherical and spherical particles, correspondingly.

Figure 6 presents the correction term ΔZ defined as

$$\Delta_1 Z_{co}(\mathrm{dB}) = \Delta Z_{co} + \Delta Z, \tag{20}$$

where ΔZ_{co} is calculated from Eq. (16) approximating enhancement observations by Marchand et al. (2013). The correction term ΔZ was estimated for the mass–size relation and characteristic particle size assumptions shown in Fig. 3. It can be seen from Fig. 6 that, while there is variability in ΔZ values based on the assumptions, the correction is rather modest, although accounting for it might be important for microphysical retrievals used with current cloud radars. For the 2.4-dB observed median value of ΔZ_{co} (Marchand et al. 2013), the correction term is around 0.7 dB.

6. Summary and discussion

Ice hydrometeors have a variety of irregular nonspherical shapes and this greatly complicates modeling ice cloud radiative effects and application of remote sensing methods for retrieving microphysical properties of such clouds (e.g., ice water content and characteristic particle size of the distribution). While experimental events, when pristine crystal shapes such as different dendritic types, plates, or columns are dominant, are sometimes observed, often pristine crystal fractions in in situ particle samples are usually not very significant (e.g., Korolev and Isaac 2003). Polarimetric radar data

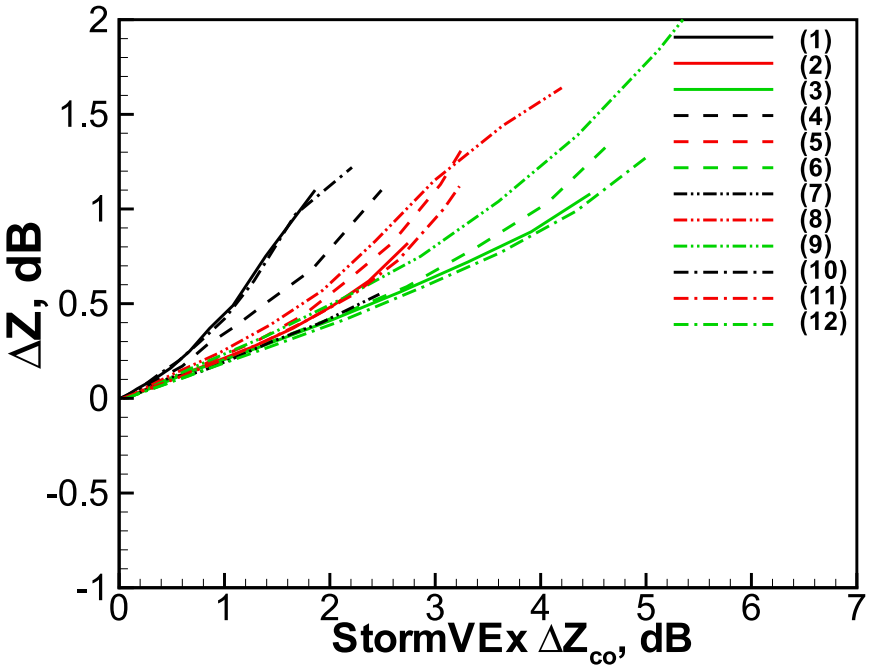

FIG. 6. Zenith enhancement correction as a function the StormVEx zenith enhancement. Curve numbers correspond the mass–size relations and D_0 values in Fig. 3.

provide ample evidence of nonspherical particle shapes influencing scattering properties of ice hydrometeor populations.

The simplest nonspherical shape used for hydrometeor modeling is that of a spheroid. It has only one parameter (i.e., aspect ratio) describing particle shapes besides a general spheroid type (i.e., oblate versus prolate). Modeling W-band depolarization ratios and zenith reflectivity enhancements of ice hydrometeor distributions characterized by varying particle mass–size relations and median volume sizes provides results that are in general agreement with observations from the scanning cloud radar in differing ice cloud and precipitation conditions.

The use of depolarization ratio (DR) measurements was evaluated for potential estimates of particle aspect ratios under the assumed spheroidal model. Unlike for the longer-wavelength polarimetric radars that transmit horizontally and vertically polarized signals and measure several polarimetric variables, DR is often the only polarimetric variable that is operationally available from many cloud radars including those operated by the DOE ARM Program. While CDR measurements are least sensitive to particle orientations and generally have higher values (i.e., stronger signals in the ''weak'' polarization receiver channel), SLDR values are expected to be similar to those of CDR when hydrometeor ''flutter'' around their aerodynamically forced preferential orientation with major dimensions in the horizontal plane is relatively small. Depolarization measurements using traditional horizontal and vertical polarizations (i.e., HLDR) show significant dependence on particle flutter (i.e., on σ_θ) and generally produce weaker cross-polarized echoes compared to SLDR. While it is feasible to reconstruct any polarization variable if full scattering matrix measurements are available in future radar systems, single depolarization measurements from current cloud radars remain a practical choice for potential retrievals of ice hydrometeor aspect ratios. From a practical standpoint, it is also often easier to implement an SLDR measurement scheme for a given radar than to convert the traditional h–v polarization basis to the circular one.

Under the oblate spheroidal model assumption, particle aspect ratios may potentially be estimated from the differences of SLDR values at slant (e.g., a 30° elevation) and zenith viewing. While these estimations do not require an assumption of homogeneous cloud layers, there is an assumption that particle habits are generally the same at slant and zenith viewing. Symmetry of elevation angle depolarization ratio trends relative to the vertical direction might be an indication of similarity of habits in a layer (even though particle concentrations may vary). Other approaches to alleviate influences of this assumption are averaging measurements from RHI scans at different azimuths or using vertical and slant

depolarization measurements with a delay tuned to the time interval required for an air parcel to be advected from a location above the radar to an approximate location corresponding to the slant viewing along the wind direction.

Errors of the aspect ratio estimations are expected to be significant. For a factor of 2 uncertainties in the particle mass–size relations and distribution characteristic size (e.g., median volume size), aspect ratios of about 0.5 ± 0.2 could be expected for the SLDR difference corresponding to the median zenith reflectivity enhancement observed by the SWACR during StormVEx. Estimated aspect ratios would represent an effective value for the whole particle size distribution. Even in presence of high estimation uncertainties, differentiating ice particles into quasi-nonspherical, moderately nonspherical, highly nonspherical, and pristine crystal categories can be useful for different practical applications. Some potential approaches to reduce aspect ratio estimate uncertainty would be using independent information about particle median sizes that could be available from dual-wavelength radar measurements that have relatively low sensitivity to bulk density assumptions (e.g., Matrosov 1998).

The relatively extensive StormVEx dataset indicated that the dominant planar hydrometeor habits were observed during a majority of experimental events, which were characterized by the increasing SLDR trend as radar viewing was changing from zenith to slant directions. The presence of columnar crystal types in mixtures, which are still dominated by planar crystals, does not significantly alter this trend (even though there could be an offset from minimal depolarization values), so SLDR changes with radar elevation angle are indicative of the dominant planar crystal aspect ratios. Rare StormVEx experimental events with a dominance of columnar crystal types were characterized by significant SLDR offsets and nearly neutral elevation angle SLDR dependencies. For these situations, a prolate spheroidal model might be appropriate for future developments of remote sensing methods of particle shape estimations.

While the use of the spheroidal bulk density model represents the simplest approach to account for nonspherical hydrometeor shapes, detailed studies of more complicated hydrometeor models with regard to their ability to replicate polarimetric properties of observed radar signals are needed in future. Potentially models resolving particle fine structures might be more successful for radar-based remote sensing of ice hydrometeor habits, especially for larger particles (e.g., $D > 5$ mm), where the ''soft'' spheroid and T-matrix method limitations are more acute and differences between various method calculations of depolarization ratios and backscatter are more pronounced (e.g., Tyynelä et al. 2011). Future studies should include comparisons of depolarization ratios obtained with the T matrix and other computational methods such as the discrete dipole approximation for the same mass and aspect ratio particles. Accounting for polarimetric cross-coupling effects is essential in comparing the computational results with radar measurements. Future microphysical research should also include more detailed studies of the correspondence between aspect ratios inferred from in situ measurements and those defined by the model.

Acknowledgments. The author thanks the StomVEx team members who participated in collecting the observational dataset.

REFERENCES

Austin, R. T., A. J. Heymsfield, and G. L. Stephens, 2009: Retrievals of ice cloud microphysical parameters using the CloudSat millimeter-wave radar and temperature. *J. Geophys. Res.,* **114,** D00A23, doi:10.1029/2008JD010049.

Avramov, A., and J. Y. Harrington, 2010: The influence of parameterized ice habit on simulated mixed-phase arctic clouds. *J. Geophys. Res.,* **115,** D03205, doi:10.1029/2009JD012108.

Bohren, C. F., and D. R. Huffman, 1983: *Absorption and Scattering of Light by Small Particles.* John Wiley and Sons, 530 pp.

Botta, G., K. Aydin, J. Verlinde, A. E. Avramov, A. S. Ackerman, A. M. Fridlind, G. M. McFarquhar, and M. Wolde, 2011: Millimeter wave scattering from ice crystals and their aggregates: Comparing cloud model simulations with X- and Ka-band radar measurements. *J. Geophys. Res.,* **116,** D00T04, doi:10.1029/2011JD015909.

Brandes, E. A., K. Ikeda, G. Zhang, M. Schonhuber, and R. M. Rasmussen, 2007: A statistical and physical description of hydrometeor distributions in Colorado snowstorms using a video disdrometer. *J. Appl. Meteor. Climatol.,* **46,** 634–650, doi:10.1175/JAM2489.1.

Bringi, V. N., and V. Chandrasekar, 2001: *Polarimetric Doppler Weather Radar.* Cambridge University Press, 636 pp.

Brown, P. R. A., and P. N. Francis, 1995: Improved measurements of the ice water content in cirrus using total-water probe. *J. Atmos. Oceanic Technol.,* **12,** 410–414, doi:10.1175/1520-0426(1995)012<0410:IMOTIW>2.0.CO;2.

Garnett, J. C. M., 1904: Colours in metal glasses and in metallic films. *Philos. Trans. Roy. Soc. London,* **203A,** 385–420, doi:10.1098/rsta.1904.0024.

Heymsfield, A. J., A. Bansemer, C. Schmitt, C. Twohy, and P. R. Poellot, 2004: Effective ice densities derived from aircraft data. *J. Atmos. Sci.,* **61,** 982–1003, doi:10.1175/1520-0469(2004)061<0982:EIPDDF>2.0.CO;2.

——, P. Field, and A. Bansemer, 2008: Exponential size distributions for snow. *J. Atmos. Sci.,* **65,** 4017–4031, doi:10.1175/2008JAS2583.1.

Hogan, R. J., and C. D. Westbrook, 2014: Equation for the microwave backscatter cross section of aggregate snowflakes using the self-similar Rayleigh–Gans approximation. *J. Atmos. Sci.,* **71,** 3292–3301, doi:10.1175/JAS-D-13-0347.1.

——, L. Tian, P. R. A. Brown, C. D. Westbrook, A. J. Heymsfield, and J. D. Eastment, 2012: Radar scattering from ice aggregates using the horizontally aligned oblate spheroid approximation. *J. Appl. Meteor. Climatol.,* **51,** 655–671, doi:10.1175/JAMC-D-11-074.1.

Holt, A. R., 1984: Some factors affecting the remote sensing of rain by polarization diversity radar in the 3- to 35-GHZ frequency range. *Radio Sci.,* **19,** 1399–1412, doi:10.1029/RS019i005p01399.

Korolev, A. V., and G. Isaac, 2003: Roundness and aspect ratio of particles in ice clouds. *J. Atmos. Sci.,* **60,** 1795–1808, doi:10.1175/1520-0469(2003)060<1795:RAARAOP>2.0.CO;2.

Leinonen, J., S. Kneifel, D. Moisseev, J. Tyynelä, S. Tanelli, and T. Nousiainen, 2012: Evidence of nonspheroidal behavior in millimeter-wavelength radar observations of snowfall. *J. Geophys. Res.,* **117,** D18205, doi:10.1029/2012JD017680.

Liu, G., 2008: Deriving snow cloud characteristics from CloudSat observations. *J. Geophys. Res.,* **113,** D00A09, doi:10.1029/2007JD009766.

Mace, G., and Coauthors, 2010: STORMVEX: The Storm Peak Lab Cloud Property Validation Experiment science and operations plan. U.S. Department of Energy Rep. DOE/SC-ARM-10-021, 53 pp.

Marchand, R., G. G. Mace, A. G. Hallar, I. B. McCubbin, S. Y. Matrosov, and M. D. Shupe, 2013: Enhanced radar backscattering due to oriented ice particles at 95 GHz during StormVEx. *J. Atmos. Oceanic Technol.,* **30,** 2336–2351, doi:10.1175/JTECH-D-13-00005.1.

Matrosov, S. Y., 1998: A dual-wavelength radar method to measure snowfall rate. *J. Appl. Meteor.,* **37,** 1510–1521, doi:10.1175/1520-0450(1998)037<1510:ADWRMT>2.0.CO;2.

——, 2007: Modeling backscatter properties of snowfall at millimeter wavelengths. *J. Atmos. Sci.,* **64,** 1727–1736, doi:10.1175/JAS3904.1.

——, R. F. Reinking, R. A. Kropfli, B. E. Martner, and B. W. Bartram, 2001: On the use of radar depolarization ratios for estimating shapes of ice hydrometeors in winter clouds. *J. Appl. Meteor.,* **40,** 479–490, doi:10.1175/1520-0450(2001)040<0479:OTUORD>2.0.CO;2.

——, A. J. Heymsfield, and Z. Wang, 2005a: Dual-frequency radar ratio of nonspherical atmospheric hydrometeors. *Geophys. Res. Lett.,* **32,** L13816, doi:10.1029/2005GL023210.

——, R. F. Reinking, and I. V. Djalalova, 2005b: Inferring fall attitudes of pristine dendritic crystals from polarimetric radar data. *J. Atmos. Sci.,* **62,** 241–250, doi:10.1175/JAS-3356.1.

——, G. G. Mace, R. Marchand, M. D. Shupe, A. G. Hallar, and I. B. McCubbin, 2012: Observations of Ice crystal habits with a scanning polarimetric W-band radar at slant linear depolarization ratio mode. *J. Atmos. Oceanic Technol.,* **29,** 989–1008, doi:10.1175/JTECH-D-11-00131.1.

Melnikov, V., and J. M. Straka, 2013: Axis ratios and flutter angles of cloud ice particles: Retrievals from radar data. *J. Atmos. Oceanic Technol.,* **30,** 1691–1703, doi:10.1175/JTECH-D-12-00212.1.

Mishchenko, M. I., L. D. Travis, and D. W. Mackowski, 1996: T-matrix computations of light scattering by nonspherical particles: A review. *J. Quant. Spectrosc. Radiat. Transfer,* **55,** 535–575, doi:10.1016/0022-4073(96)00002-7.

Mitchell, D. L., 1996: Use of mass- and area-dimensional power laws for determining precipitation particle terminal velocities. *J. Atmos. Sci.,* **53,** 1710–1723, doi:10.1175/1520-0469(1996)053<1710:UOMAAD>2.0.CO;2.

Petty, G. W., and W. Huang, 2010: Microwave backscatter and extinction by soft ice spheres and complex snow aggregates. *J. Atmos. Sci.,* **67,** 769–787, doi:10.1175/2009JAS3146.1.

Pruppacher, H. R., and J. D. Klett, 1978: *Microphysics of Clouds and Precipitation.* D. Reidel, 714 pp.

Reinking, R. F., S. Y. Matrosov, R. A. Kropfli, and B. W. Bartram, 2002: Evaluation of a 45° slant quasi-linear radar polarization for distinguishing drizzle droplets, pristine ice crystals, and less regular ice particles. *J. Atmos. Oceanic Technol.,* **19,** 296–321, doi:10.1175/1520-0426-19.3.296.

Tyynelä, J., and V. Chandrasekar, 2014: Characterizing falling snow using multifrequency dual-polarization measurements. *J. Geophys. Res. Atmos.,* **119,** 8268–8283, doi:10.1002/2013JD021369.

——, J. Leinonen, D. Moisseev, and T. Nousiainen, 2011: Radar backscattering from snowflakes: Comparisons of fractal, aggregate and soft spheroid models. *J. Atmos. Oceanic Technol.,* **28,** 1365–1372, doi:10.1175/JTECH-D-11-00004.1.

Zrnić, D., R. Doviak, G. Zhang, and A. Ryzhkov, 2010: Bias in differential reflectivity due to cross coupling through the radiation patterns of polarimetric weather radars. *J. Atmos. Oceanic Technol.,* **27,** 1624–1637, doi:10.1175/2010JTECHA1350.1.